journal

J. Am. Ceram. Soc., 75 [10] 2733–41 (1992)

Exaggerated Texture and Grain Growth in a Superplastic SiAlON

Xin Wu* and I-Wei Chen*

Department of Materials Science and Engineering, University of Michigan, Ann Arbor, Michigan 48109–2136

A fine-grained superplastic β′-silicon nitride solid solution (SiAlON) was found to develop elongated grains and a pronounced texture during tensile deformation at 1550°C. The texture development is well-described by a geometrical model of grain rotation in accordance with the strain field. Once aligned, grains can then grow with little constraint due to impingement and often coalesce into each other. With the above microstructural development, the stress–strain curve displayed unusually strong strain hardening characteristics due to a fiber-reinforcement effect of the aligned silicon nitride grains on the glass-containing matrix. By extending the rheological model of Chen and Yoon and considering these microstructural evolutions, we are able to simulate the deformation behavior.

I. Introduction

Superplastic ceramics with a characteristic fine-grained microstructure often manifest unique dynamic behavior during large strain deformation. For example, strain-induced dynamic grain growth,[1] which can be correlated to the grain boundary mobility, has been established in many superplastic ceramics, most notably zirconia and alumina. (For a review, see Ref. 2.) Although a liquid phase may enhance dynamic grain growth in this case, it does not seem to be necessary for the occurrence of that phenomenon. On the other hand, a novel shear-thickening transition has been recently reported in a large family of superplastic silicon nitride in which the liquid phase does play a central role.[3] Here we report yet another observation on a liquid-enhanced texture and grain morphology development during large tensile deformation of a superplastic silicon nitride. The resultant microstructure, with highly elongated β-silicon nitride grains aligned along the tensile axis, gives rise to an exceptionally high ductility at 1550°C. This is contrary to the common experience of the deleterious effect of anisotropy and texture on superplasticity.

The study of the microstructural development of β-silicon nitride with elongated grains has received renewed interest in recent years.[4–9] This is because of the realization that grain size, grain shape, and grain orientation have a very strong effect on the mechanical properties. These studies indicate that an elongated, prismatic grain shape can be developed during sintering, hot-pressing, or annealing if a high temperature (above 1700°C), and especially if a nitrogen overpressure, are employed.[4,8,9] The present study on superplastic flow and the attendant microstructural development at a much lower temperature (1550°C) has provided a counterexample which could prove enlightening on this subject.

D. S. Wilkinson—contributing editor

Manuscript No. 196103. Received December 27, 1991; approved May 21, 1992.
Supported by the U.S. Department of Energy (BES) under Grant No. DE-FG02-87ER45302.
*Member, American Ceramic Society.

II. Experimental Procedure

(1) Material and Specimen Preparation

A glass-phase-rich yttria-doped silicon nitride (β′-SiAlON), 0.2Y:6.4Si:5.6Al:5.0O:11.0N, was processed by the following procedure. A powder mixture of 52.6 wt% α-Si_3N_4 (E10, UBE, Tokyo, Japan), 17.3 wt% AlN (Dow Chemical Company, Midland, MI), 26.3 wt% Al_2O_3 (AKP-50, Sumitomo Chemical Co., Ltd., Tokyo, Japan), and 3.8 wt% Y_2O_3 (99.99%, Aldrich Chemical Company, Inc., Milwaukee, WI) was attrition-milled for 2 h in isopropyl alcohol using Al_2O_3 balls of about 3 mm in diameter. The slurry was dried, and the powder was hot-pressed into a 35 mm × 34 mm × 2.5 mm plate using a graphite die and in a graphite resistance furnace. Hot-pressing was performed at 35 MPa and at 1550°C for 30 min in static nitrogen of 1 atm, followed by cooling at a rate of 15°C/min to below 1000°C. The hot-pressed plates were machined to tensile specimens with a surface grinder and diamond wheels. The dimensions of the gauge section were 14 mm in length, 3 mm in width, and 2 mm in thickness.

(2) Tensile Test

Tensile tests were performed in an environmental furnace with a tungsten heating element, in flowing nitrogen of 1 atm. The furnace has a hot zone 200 mm in length and 85 mm in diameter, which has a sufficiently uniform temperature distribution for superplastic extension of the specimens used here. Temperature was measured by a C-type thermocouple (W–5%Re vs W–26%Re) and controlled by a programmable temperature controller to within 1°C of the set temperature. The temperature was also monitored by an optical pyrometer through a side window.

A pair of high-temperature tensile grips, made of hot-pressed SiC rods, was used. The tensile load was applied on the specimen's shoulder by edge contact with the grip. A layer of graphite foil, 0.05 mm in thickness, was placed between the specimen and the grip to prevent possible chemical reaction. Since the cross-sectional area of the shoulder section is much larger than that of the gauge section, the deformation in the shoulder section is negligible.

Tensile tests were performed at constant temperatures of 1535°, 1550°, 1565°, and 1580°C, using a servohydraulic mechanical tester, which has both stroke- and load-controlling functions and an automated data acquisition system. Most of the tests were at constant displacement rates (V = 0.00042 to 0.014 mm/s) equivalent to initial strain rates $\dot{\varepsilon}_0$ in the range of 3×10^{-5} to 1×10^{-3} s^{-1}. To measure the strain rate sensitivity, additional tensile tests with variable speeds were also performed at 1550°C. The procedure we used involved both step speed increase and step speed decrease in a single test, and the average flow stress and strain rate are reported here.

After each tensile test, which was terminated upon specimen fracture or when a certain deformation stage was reached, the furnace power was immediately turned off. The temperature then dropped rapidly to below 1000°C within a few minutes.

(3) Microstructural Examination and Texture Evaluation

Fracture surfaces and microstructures were examined in a scanning electron microscope (SEM) using Au–Pt coated specimens. To reveal grain boundaries, the sectioned specimens were polished to a 0.5-μm diamond finish. They were then etched by immersion in a molten hydroxide mixture composed

of LiOH:2NaOH:2KOH (in weight ratio), for about 10 s, followed by soaking in nitric acid to remove any residual hydroxide. In some cases, an additional thermal etching step was introduced before molten salt etching to better reveal the grain boundaries.

Microstructural and textural examinations were generally performed in both the longitudinal (tensile) direction (L) and the transverse direction (W) for the deformed specimens. Since an elongated grain shape and a preferred orientation were also observed for the deformed specimens, three parameters were used to characterize the microstructure obtained on the sectioned surfaces. They are the maximum and minimum dimensions of each sectioned grain, denoted by ℓ and w respectively or by an aspect ratio $a = \ell/w$. In addition, the grain orientation angle ψ is taken to be that between the long axis ℓ and the tensile direction ($0 \leq \psi \leq \pi/2$). Measurements of ℓ and ψ, for individual grains that lay entirely within the photographed areas of longitudinally sectioned surfaces, were averaged over more than 100 grains. The grain width w was measured on both longitudinally and transversely sectioned surfaces, which gave nearly indistinguishable results. It is recognized that the above method for determining ℓ, w, and ψ relies on 2-D sectioning of a 3-D microstructure in which a certain systematic error has been introduced, i.e., an underestimation of the aspect ratio. However, for a strongly oriented microstructure, as is the case here, the error is relatively small, and the reported data are still informative.

The volume fraction of the intergranular phase was determined from the area fraction of the bright region on a SEM image of a polished surface without etching. This is possible because yttrium, being the strongest electron-emitting element in this system, has no solubility in SiAlON and is thus segregated into the intergranular phase, giving rise to a bright contrast in the latter. Lastly, to identify phases and crystallographic texture, X-ray diffraction (XRD) analysis, using Cu$K\alpha$ radiation, was performed. Estimation of phase fractions in the untextured specimens was made by comparing XRD peak height ratios.

III. Results

Figure 1 shows a tensile specimen with an elongation δ = 230% (true strain = 1.2), tested at 1550°C and a displacement rate V = 0.0014 mm/s, or an initial strain rate $\dot{\varepsilon}_0 = 10^{-4}\ s^{-1}$. (Hereafter, the strain rates given all refer to the initial values.) The specimen had uniform deformation over its entire gauge section and did not fail when the test was terminated. The stress–strain data of this test along with two others are shown in Fig. 2 in diamonds. At $\dot{\varepsilon}_0 \leq 10^{-4}\ s^{-1}$, the flow stress is very low initially, and then increases continuously. By the end of the test, it has increased by more than a factor of 10, despite a decrease in the strain rate by a factor of three due to the lengthening of the gauge section. The same observation was found in other tests at even lower strain rates, sometimes with a flow stress increase of more than a factor of 20, as seen in Fig. 2. However, at faster strain rates, e.g., $3 \times 10^{-4}\ s^{-1}$, the stress–strain curve is essentially flat. Nevertheless, a large elongation was still obtained, for example, 70% (ε = 0.53) after 38 min in one case. Also shown in Fig. 2 are model predictions for the stress–strain curves which will be discussed in Section IV(3).

The initial flow stresses, taken at the beginning of the steady-state deformation after the loading transient following each speed change, are shown in Fig. 3. From these data, the rate sensitivity m was calculated to be 0.68, and thermal activation energy Q to be 940 kJ/mol, based on the constitutive equation

$$\dot{\varepsilon} = A\sigma^n \exp(-Q/RT) \qquad (1)$$

where $n = 1/m$.

These values are typical for superplastic silicon nitride systems.[3,10] The elongations vs strain rates and temperatures are plotted in Fig. 4, which shows the best superplastic condition to be at 1550°C and at strain rates lower than $10^{-4}\ s^{-1}$.

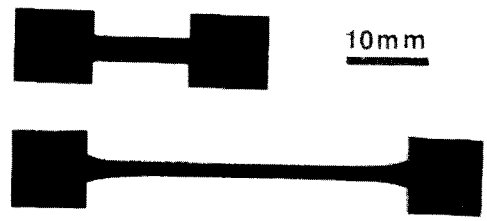

Fig. 1. A β′-SiAlON specimen with 230% elongation, tested at 1550°C and a displacement rate of 0.0014 mm/s ($\dot{\varepsilon}_0 = 10^{-4}\ s^{-1}$).

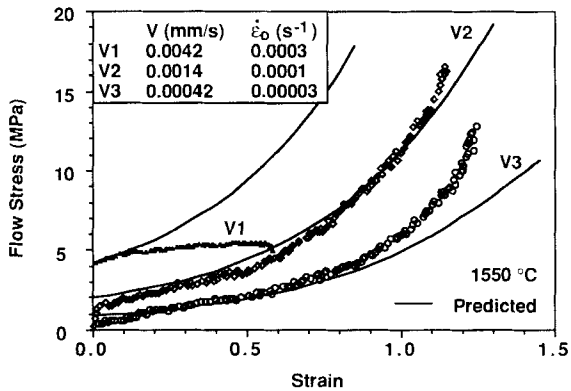

Fig. 2. Typical tensile stress–strain curves showing pronounced strain hardening at low strain rates and no strain hardening at high rates. Also shown in solid curves are model predictions (see text).

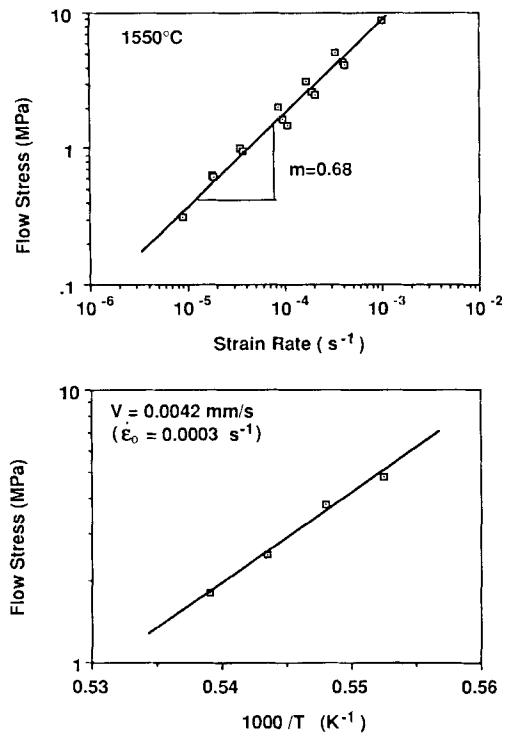

Fig. 3. Initial flow stress vs strain rate (top) and temperature (bottom).

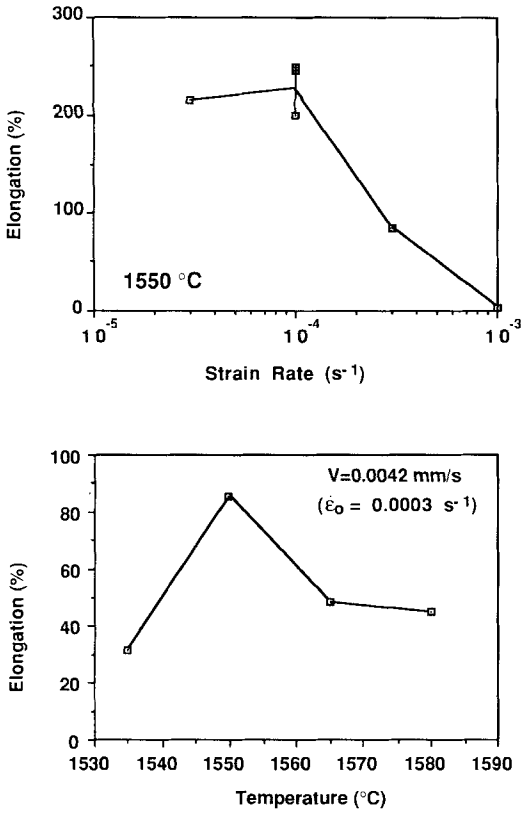

Fig. 4. Elongation vs initial strain rate (top) and temperature (bottom).

The microstructure of a specimen hot-pressed at 1550°C for 30 min is presented in Fig. 5(A). It features many fine grains of a size of about 0.35 μm. These grains do not appear very elongated on the sectioned plane, and their distribution is quite uniform. After the same specimen was annealed at 1550°C for 18 h, its microstructure coarsened to a grain size of 0.8 μm, with some elongated grains appearing, as shown in Fig. 5(B). On the other hand, deformation caused a profound change in the microstructure. Figures 6(A) and (B) show a specimen with $\delta = 246\%$ ($\varepsilon = 1.24$, $V = 0.0014$ mm/s, and $\dot{\varepsilon}_0 = 1 \times 10^{-4}$ s^{-1}, for about 6 h) sectioned in the L and W directions. The grains have become elongated, with their long axes preferentially aligned along the tensile axis. Interestingly, however, these grains do not have a regular prismatic shape, as is usually observed for this material family.[4-9] Indeed, their boundaries are often curved, with variable diameters along their lengths.

To illustrate the development of grain alignment, the mean grain orientation angle ψ was measured at different strains. The mean value of ψ shown in Fig. 7 clearly decreases. Grain orientation distribution functions (ODF) have also been measured for several samples, and one of them is shown in the inset of Fig. 7. The accompanying development of the grain size parameters, ℓ, w, and a, plotted in Fig. 8, reveals a linear increase in ℓ at a rate which is strain-dependent but rate-independent. Also significant is the finding that the growth in w was relatively small, thus resulting in a linear increase of the aspect ratio. When normalized by the initial grain size, the highest grain growth rate observed on the long axis was around 10^{-4} s^{-1}, compared to the static grain growth rate of 2×10^{-5} s^{-1} measured at the same temperature, as indicated by the grain size marked as annealed on Fig. 8.

The crystallographic orientation of the long axis of the grains in the deformed specimens was identified by XRD. The results as examined along the L and W directions are shown in Fig. 9(A). (This specimen is the same one shown in Fig. 1, and the reflections of silicon nitride have been indexed.) It shows a very strong texture, as can be seen from a comparison of the intensity ratio of the Si_3N_4 (002) and (200) peaks along the L and W directions. This texture, along with the elongated microstructure shown in Figs. 6(A) and (B), identifies the grain axis as along [002]. For comparison, the XRD spectra from the shoulder section are also shown in Fig. 9(B). The latter were found to be essentially the same as the ones obtained for the undeformed specimens with a very weak crystallographic texture inherited from hot-pressing which did not seem to develop any further during annealing.

The XRD spectra specimen revealed the following phase assemblage: β'-$Si_{6-x}Al_xO_xN_{8-x}$ (β'-SiAlON), 15R (an AlN polytype), and $Y_3Al_5O_{12}$ (YAG). Although both β'-SiAlON and the polytype were found to be textured, the YAG was not, since it has a cubic crystal structure which is commonly believed to crystallize from the glassy melt during cooling. Indeed, we found the YAG peaks to be considerably stronger in the shoulder section than in the gauge section, consistent with a much slower cooling rate in the former due to the large thermal mass of the grip. (The YAG (211) reflection at $2\theta = 18.1°$ can be used to easily identify the phase, since it does not overlap with either Si_3N_4 peaks or 15R peaks.) Therefore, the total amount of the glassy phase with YAG inclusions, which constituted about 20 vol%, was independently estimated from metallography. (See the dark, etched-out regions in Figs 4(A,B) and Fig. 6(B)). This value remained unchanged before and after tensile deformation. The SiAlON and 15R constitute the remaining 80 vol%.

A further analysis of the SiAlON reflections allowed us to determine the composition of $Si_{6-x}Al_xO_xN_{8-x}$, using the correlation between lattice parameters and x published in the literature.[11] This generally placed x at around 3.0 in both the as-hot-pressed and 1550°C heat-treated/tested specimens. We also found that x decreased slightly with time at 1550°C while the amount of YAG increased concurrently, probably due to the slow oxidation which, in turn, increased the amount of the glassy phase. Nevertheless, these microchemical changes were rather small and did not significantly affect the volume fraction of the glassy phase.

Figure 10 shows the fractured surfaces of two specimens tested at 1550°C. Specimen (A) was tested at a faster rate ($V = 0.014$ mm/s or $\dot{\varepsilon}_0 = 10^{-3}$ s^{-1}) and failed at an elongation of 3%, with the fracture stress reaching 7 MPa. Specimen (B) was tested at a slower rate ($V = 0.0014$ mm/s or $\dot{\varepsilon}_0 = 10^{-4}$ s^{-1}) and failed at $\delta = 246\%$, with the stress reaching 18 MPa. Although both specimens fractured intergranularly, the morphology of the two are quite different: specimen (A) fractured with equiaxed grains exposed, since no texture was developed during the very short test time, whereas specimen (B) shows elongated grains aligned normal to the fractured surface. The latter is reminiscent of the fracture surface appearance in fiber-reinforced composites when "fiber pullout" occurs. This aspect, along with the microstructural development, will be analyzed in the next section.

IV. Theoretical Analysis

(1) Texture Development

A simple geometrical model for the rotation of elongated grains during tensile straining is first described. A shape anisotropy is assumed to exist from the start or soon after the deformation ensues. This assumption seems justified for β'-SiAlON, which has a tendency for anisotropic grain growth.[4-9] Texture is generally described by a three-dimensional (3-D) orientation distribution function (ODF) of three independent angular variables, such as the three Eulerian angles.[11] The axisymmetry of tensile deformation, however, simplifies the ODF to be expressed in one variable only. This function is denoted by $f(\phi)$, where $0 \leq \phi < \pi/2$ is the angle between the grain long axis and the tensile L axis in 3-D. We will also introduce the subscript "$_0$" to denote quantities pertaining to the initial state of the material.

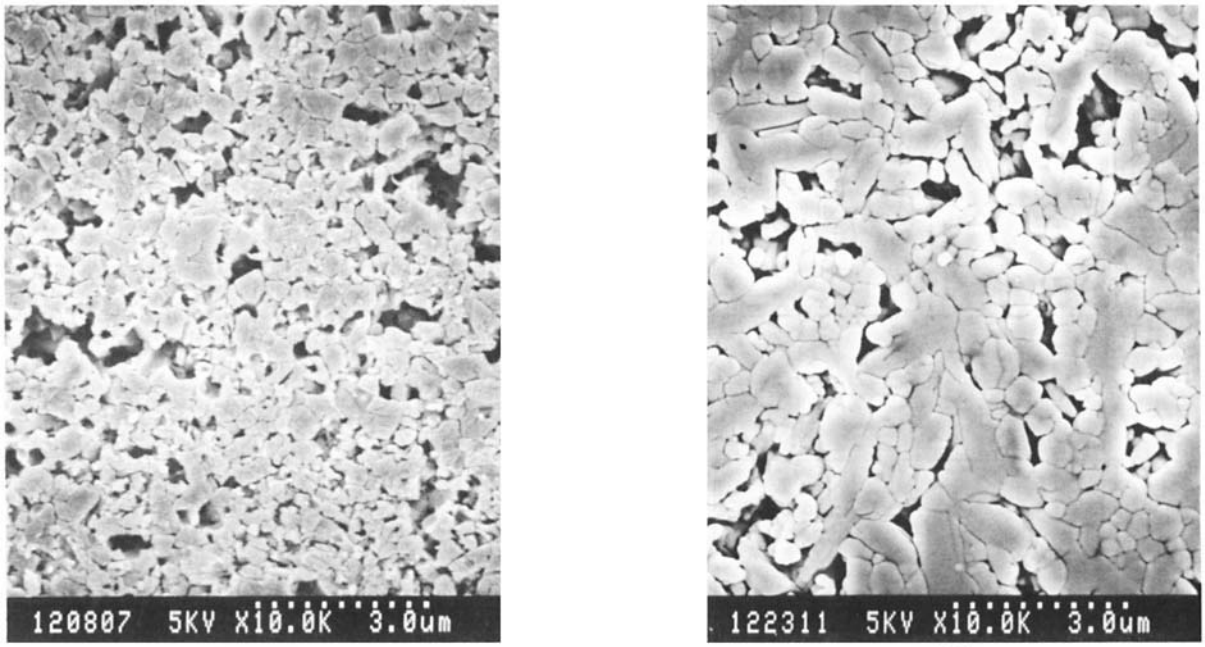

Fig. 5. SEM micrographs of a specimen (A) hot-pressed at 1550°C for 30 min and (B) after annealing at 1550°C for 18 h.

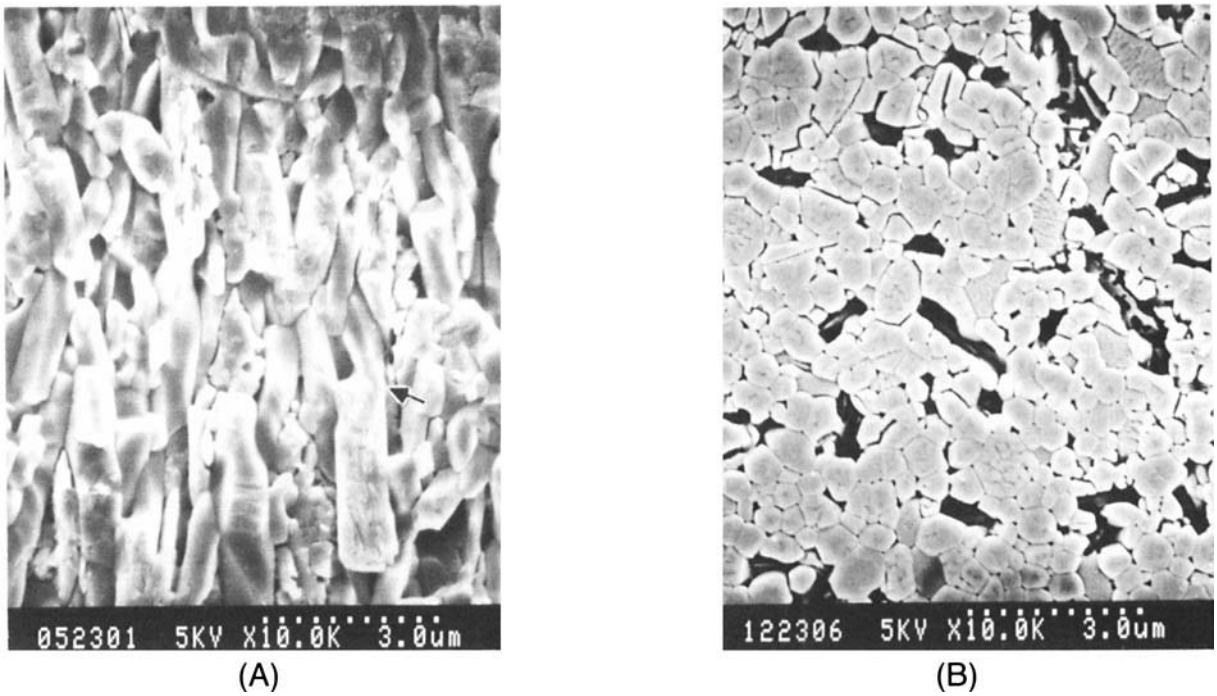

Fig. 6. SEM micrographs of a specimen after tensile deformation at 1550°C, $\dot{\varepsilon}_0 = 10^{-4}\ s^{-1}$, to $\delta = 246\%$, sectioned (A) parallel (L) and (B) perpendicular (W) to the tensile direction.

For an initially random distribution of grains, the probability for a grain to be oriented within ϕ_0 from the tensile axis is simply computed from the ratio of the surface area of a crown extended from the pole to an angle ϕ below, over that of a hemispherical dome. Thus,

$$F_0(\phi_0) = 1 - \cos \phi_0 \qquad (0 \leq \phi_0 < \pi/2) \tag{2}$$

By differentiation one can obtain the orientation distribution function as

$$f_0(\phi_0) = \frac{d}{d\phi_0} F_0(\phi_0) = \sin \phi_0 \tag{3}$$

Note that the above ODF is not constant over ϕ. Referring to Fig. 11, a tensile strain ε stretches a volume element of a dimension $x_0 \cdot x_0 \cdot y_0$ to $x \cdot x \cdot y$. Then, for a grain which is initially situated along the diagonal of the volume element $x_0 \cdot x_0 \cdot y_0$, there is a tendency for it to rotate during stretching. If the rotation is totally unimpeded, as would be the case for a rod in a viscous liquid, the rotation from ϕ_0 to ϕ is prescribed by the following geometric relationship:

$$\frac{\tan \phi}{\tan \phi_0} = \frac{x/y}{x_0/y_0} = \exp(-1.5\varepsilon) \tag{4}$$

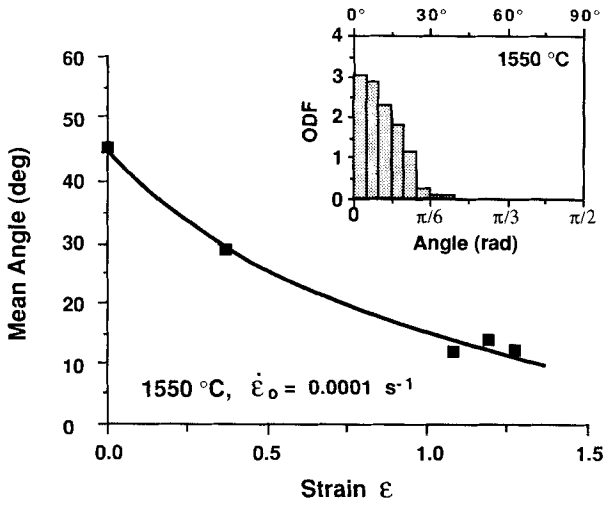

Fig. 7. Mean grain alignment orientation vs tensile strain. The orientation distribution function at $\varepsilon = 1.2$ is shown in the inset.

or

$$\phi_0 = \tan^{-1}[\exp(1.5\varepsilon)\tan\phi] \tag{5}$$

Lastly, noting that the probability of a grain aligned within ϕ_0 at $\varepsilon = 0$ is the same as that within ϕ after a strain ε, we obtain from Eqs. (2,5)

$$F(\phi,\varepsilon) = F_0(\phi_0) = 1 - [1 + \tan^2\phi\exp(3\varepsilon)]^{-1/2} \tag{6}$$

Thus, the new distribution function in terms of the current orientation is

$$f(\phi,\varepsilon) = \frac{\partial}{\partial\phi}F(\phi) = \exp(3\varepsilon)[1 + \tan^2\phi\exp(3\varepsilon)]^{-3/2} \times \tan\phi\sec^2\phi \qquad (0 \le \phi \le \pi/2) \tag{7}$$

In order to compare this model with the experimentally measured grain orientation angle on a longitudinal cross section, the 2-D projection of the solid angle ϕ on a plane parallel to the tensile axis is needed. Now denote ψ as the angle between the grain long axis and the tensile axis on the 2-D projection (the same ψ was used in the experimental measurements for grain orientation), and $g(\psi,\varepsilon)$ as the corresponding distribution function. It can be shown that the initial random distribution yields a

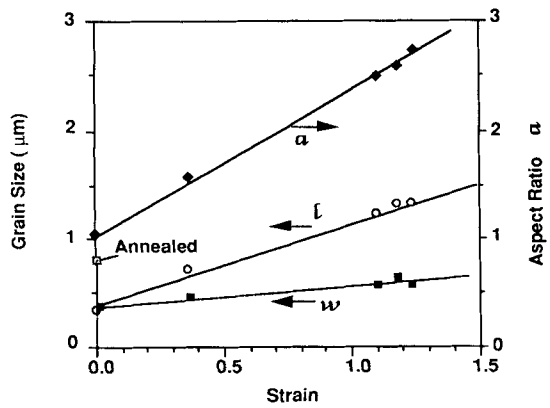

Fig. 8. Grain length ℓ, width w, and aspect ratio a, vs strain. The grain size obtained after annealing at 1550°C for 18 h without deformation is also shown as marked.

$g_0(\psi_0)$ which is independent of ψ. (All the 3-D orientations, lying on a great circle that contains both the normal of the projected plane and the direction vector ψ_0 on the plane, have the same projected direction as ψ. These circles are all of the same size, regardless of ψ; hence the constancy of $g_0(\psi_0)$.) Therefore,

$$g_0(\psi_0) = 2/\pi \qquad (0 \le \psi_0 \le \pi/2) \tag{8}$$

The probability for a measured grain to lie within ψ_0 is then

$$G_0(\psi_0) = 2\psi_0/\pi \tag{9}$$

Since an equation similar to Eq. (5) also holds for the set of angles ψ and ψ_0, we can follow the same argument from Eq. (5) to Eq. (6) to write

$$G(\psi,\varepsilon) = G_0(\psi_0) = \frac{2}{\pi}\tan^{-1}[\exp(1.5\varepsilon)\tan\psi] \tag{10}$$

giving the ODF of the 2-D projection

$$g(\psi,\varepsilon) = \frac{\partial}{\partial\psi}G(\psi,\varepsilon) = \frac{2}{\pi}\exp(1.5\varepsilon)[\cos^2\psi + \sin^2\psi\exp(3\varepsilon)]^{-1} \tag{11}$$

This function will next be used for a direct comparison with the experimental data.

The calculated orientation distribution and its 2-D projection, Eqs. (7) and (11), are plotted in Fig. 12 for $\varepsilon = 1.2$. Also plotted are the mean orientation angles, which are computed by integrating $\psi g(\psi)$ and $\phi f(\phi)$ over 0 to $\pi/2$, as a function of strain. Comparing Fig. 7 with the predicted 2-D ODF and mean angle, we find that they are in obviously good agreement. (In principle, the 3-D ODF could be directly verified by X-ray pole figures or ODF measurements, which were not attempted here.) This agreement suggests that our geometrical model is reasonable and that grain reorientations in a viscous liquid are not impeded in the present experiment.

(2) Strain-Induced Grain Growth

Our experimental results have indicated simultaneous grain growth during deformation, which is absent in hot-pressing and static annealing. (Shear) strain is thus an important element for grain growth. The micrograph presented in Fig. 6 further reveals that the enhanced growth produces a highly unusual grain shape with curved boundaries instead of the flat facets commonly observed in β-silicon nitride. The morphology above strongly suggests an important role of grain coalescence. We envision this to take place with the aid of grain reorientation which brings two adjacent grains into near axial alignment. A further rotation around the long axis of the grain can then bring these two grains into crystallographic registry. (Because of hexagonal symmetry, the relative rotation never needs to exceed 30°.) The two grains can now be welded into one, with a twofold increase in the aspect ratio. At this point, if the two grains have not lined up on any of their side faces, a jagged step will remain after grain coalescence which can only be smoothed out in time by diffusion. The latter process occurs relatively rapidly when the grain size is small. For longer grains that are prevalent at larger tensile strains, diffusional smoothing becomes difficult due to the longer diffusion distance. This should then give rise to a wavy appearance on the side faces, as observed in Fig. 6. The above growth mechanism is obviously of little importance without tensile deformation, which brings grains into alignment in the first place. Thus, the growth is entirely strain-induced and its extent depends only on the strain. (Grain coalescence in liquid phase sintering has been treated before, e.g., Ref. 13, but the effect of strain and grain alignment has not.)

In addition to the above, we suggest that grain reorientation may enhance grain growth by modifying the stress state in the grain assemblage for the following reason. This contribution can best be pictured as a strain-induced grain unimpingement

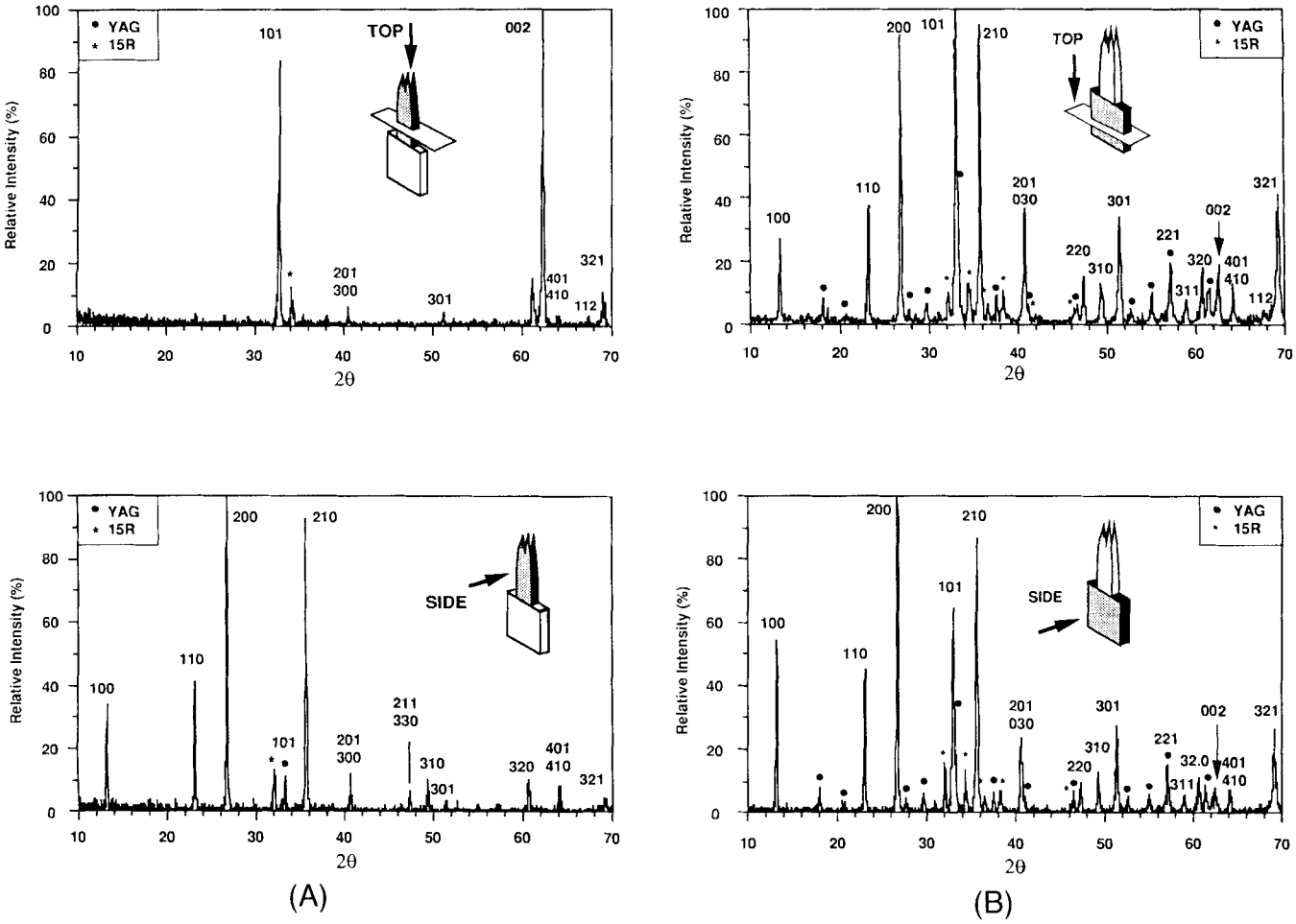

Fig. 9. XRD patterns of a specimen tested at 1550°C, $\dot{\varepsilon}_0 = 10^{-4}\ s^{-1}$, $\delta = 246\%$, in (A) two directions from the gauge section and (B) two directions from the shoulder section. Only reflections of Si_3N_4 are indexed. Reflections of other phases are indicated by symbols ★ (15R) and ● (YAG) for clarity.

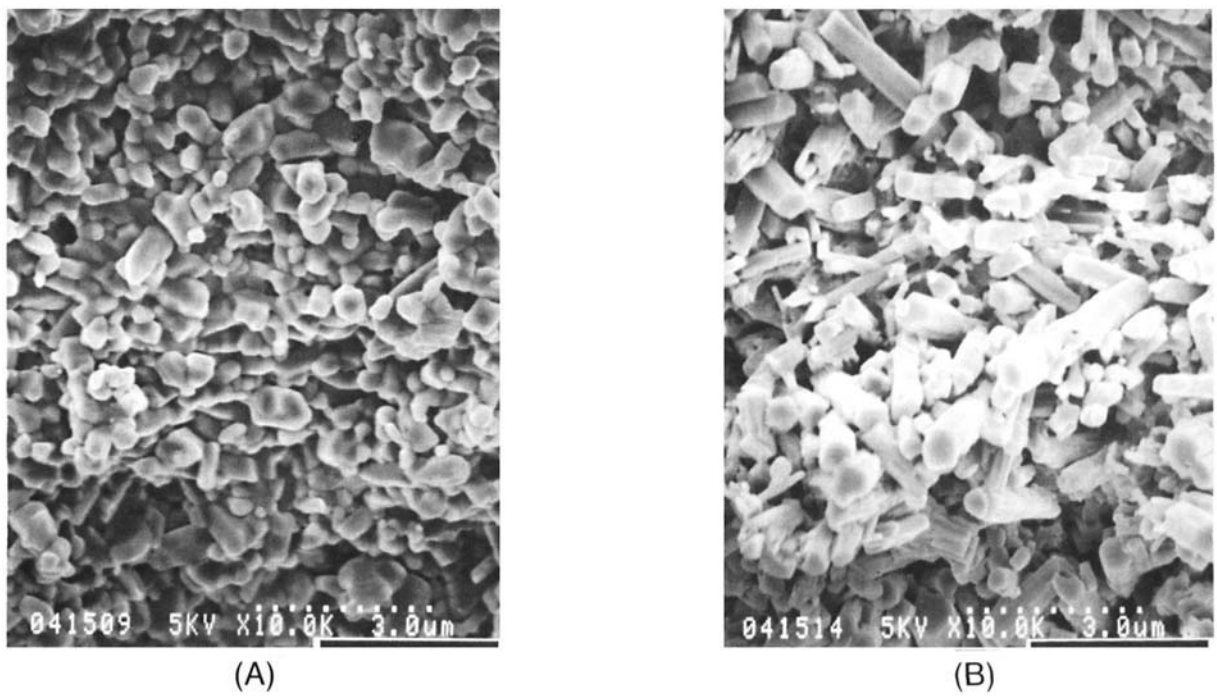

Fig. 10. SEM micrographs of the fracture surfaces of two specimens tested at 1550°C. (A) $\dot{\varepsilon}_0 = 10^{-3}\ s^{-1}$, $\delta = 3\%$; (B) $\dot{\varepsilon}_0 = 10^{-4}\ s^{-1}$, $\delta = 246\%$.

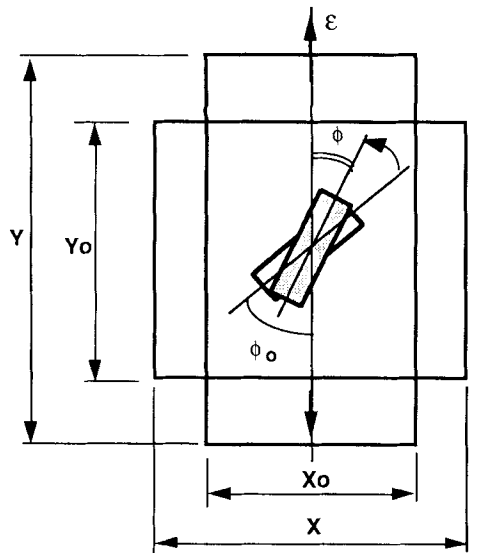

Fig. 11. A schematic of grain rotation due to large strain deformation.

process. Essentially, static grain growth in silicon nitride as an Ostwald ripening process[14] proceeds by a mass transport through the liquid silicate phase. Unlike solid-state grain growth, in which the mass transport involves atoms rearranging at the grain boundary and does not necessitate any net strain locally or macroscopically, grain growth of silicon nitride will probably entail a local volume increase at the growing grains and vice versa at the shrinking grains. The resultant local strain gradient can usually be relieved by the liquid flow. Under static growth conditions, however, grains eventually impinge on each other and become interlocked. Further growth is now very sluggish, since the growth constraint can no longer be easily relieved by the liquid. The situation is accentuated by anisotropy in the grain shape which makes grain interlocking more likely. During deformation, this interlocking constraint can be removed if the impinging grains are pulled apart by grain alignment. More specifically, growth can resume if the local axial strain along the grain is tensile. By performing a coordinate transformation for the strain rate tensor $\dot{\varepsilon}_{ij}$ (where ij = 1,2,3, and 1 is in the tensile direction), we find the strain rate along the grain axis (direction ϕ) to be

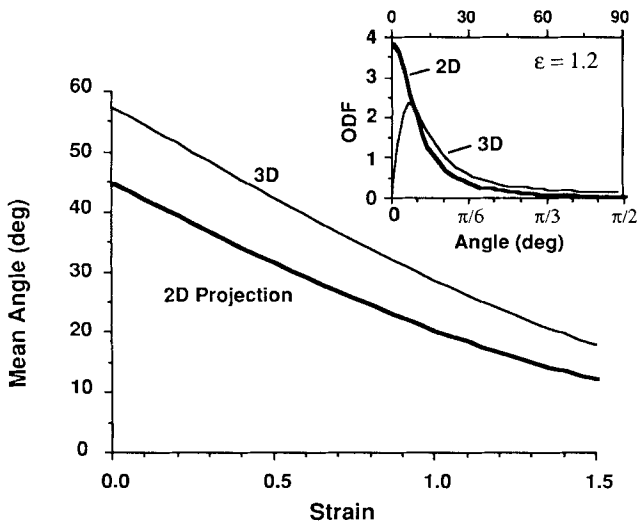

Fig. 12. Predicted mean grain orientation vs strain and the orientation distribution function (inset). Both the actual orientation with respect to the tensile axis (3-D) and the projected orientation on a section parallel to the tensile axis (2-D) are shown.

$$\dot{\varepsilon}_\phi = \frac{1}{2}(3\cos^2\phi - 1)\dot{\varepsilon} \tag{12}$$

where $\dot{\varepsilon}$ is the macroscopic strain rate in the tensile test. Thus, grains lying within a critical angle $\phi_c = \cos^{-1}(1/\sqrt{3})$ ($\approx$57°) will have a local tensile axial strain component that effects unimpingement and releases the constraint. As tensile deformation continues, more and more grains will be placed within such a favorable orientation and experience less constraint. Through this mechanism, strain-enhanced grain growth is once again expected.

(3) Flow Behavior

We now estimate the flow stress enhancement of the present glass-containing β′-SiAlON as a result of microstructural development. For this task, we will use a rheological model for the composite which we previously developed.[15,16] We first assume that the matrix phase (intergranular viscous liquid phase) is "soft" and obeys a flow equation of the form

$$\dot{\varepsilon} = \dot{\varepsilon}_0(\sigma/\sigma_0)^n \tag{13}$$

where $\dot{\varepsilon}_0$ and σ_0 are reference strain rate and stress. Grains of β′-SiAlON, which constitute a volume fraction v, are considered to be rigid. The composite strain rate $\dot{\varepsilon}$ at a stress σ is then[16]

$$\dot{\varepsilon} = \dot{\varepsilon}_0(1 - v)^q(\sigma/\sigma_0)^n \tag{14}$$

where q may be identified as a stress concentration factor for the rigid phase. In our case, the stress concentration depends on the aspect ratio a and the orientation angle ϕ of the grain. For grains aligned in the tensile direction, a shear-lag analysis such as the one performed in Ref. 16 can be quoted to give $q = q_{//} = 1 + (1 + n/2)a$. In the other extreme, for grains aligned transversely to the tensile axis, the same reference which found the grain shape effect unimportant can again be quoted to give $q = q_\perp = 1 + (1 + n/2)$. If we now take the weighted average of the two extremes, the approximate stress concentration factor for a grain at an angle ϕ becomes

$$q(\phi) = \cos\phi q_{//} + \sin\phi q_\perp \tag{15}$$

In the same spirit, the orientation average is taken to be

$$q_{\text{eff}}(\varepsilon) = \int_0^{\pi/2} q(\phi) f(\phi, \varepsilon)\, d\phi \tag{16}$$

where the ODF from Eq. (7) is used and an additional strain dependence in q is also introduced to allow for the changing aspect ratio with tensile deformation. The above q_{eff} is used to substitute for q in Eq. (14) to obtain the overall reinforcement effect. By taking $v = 0.8$ and $m = 1/n = 0.68$, and using the initial flow stress data of (σ, $\dot{\varepsilon}$) from Fig. 3 when the anisotropy is limited ($q_{\text{eff}} = 2 + n/2$), the flow behavior of the composite as a function of strain can be simulated in the form of a stress–strain curve. This is shown in Fig. 2 as solid curves for three displacement rates. As can be seen, except at the highest strain rate, our model correctly predicts the unique shape of the stress–strain curves by resorting to the in situ "fiber reinforcement" effect as the source of strain hardening. This strengthening effect is accelerating with strain because of the increasing degree of grain alignment and shape anisotropy. The exception at the highest strain rate, which is due to the inadequate time for growing sufficiently elongated grains, will be discussed in Section V(3).

V. Discussion

(1) Ductility and Whiskerlike Microstructure

The elongation achieved here is quite high and is especially unusual for a textured material with an elongated hard second phase. Past experience in whisker addition to superplastic materials (SiC whiskers to ZrO_2, for example[17]) has always

resulted in a severe loss of ductility. Dynamic grain growth has a similar consequence on fine-grained ceramics and renders them much less ductile (Al_2O_3,[2,18,19] Ce-TZP,[2,20] and cubic zirconia,[2] for example). The results here are just the contrary. The cause for this anomaly is discussed below.

For (superplastic) ceramics deformed at high temperatures, elongation is not limited by necking, as is often observed for metallic materials, but by interfacial decohesion.[2] Thus, a lower flow stress relative to the interfacial (grain boundary) decohesion stress should lead to a higher elongation,[2] and generally the ductility decreases monotonically with strain rate. For the same reason, strain hardening is detrimental to achieving tensile ductility in ceramics. In the present case, however, the situation is modified by the microstructural development which continually raises the flow stress during deformation (by load transfer) to the hard inclusions which are capable of higher stresses when they become more elongated. Thus, although the ductility–initial strain rate (or flow stress) correlation, as shown in Fig. 4, follows an inverse relationship common to other superplastic ceramics,[2] a very high flow stress is reached by the time of fracture after a large elongation. Premature failure in these cases is prevented because an increasing portion of the flow stress is carried by the side surfaces of the elongated grains in the form of shear traction, which transfers a large tensile stress to the midsection of the whisker. Meanwhile, the normal stress at the whisker's end is kept low as dictated by the low flow stress of the viscous liquid phase. Inasmuch as no large normal stresses exist anywhere at the whisker–liquid interface, interfacial decohesion can be prevented. Thus, the grain alignment and grain shape anisotropy are beneficial attributes in this case.

Actually, the fracture could also be delayed for another geometrical reason. This is because, in a textured microstructure with elongated grains, cavitating facets are displaced from each other by a half-length of the (elongated) grain and, as in the case of a "bamboolike" microstructure, they would have more difficulty in linking up with each other. Thus, the development of the unique microstructure probably also enhances the ductility.

It is interesting to compare the above microstructure/strength/ductility relationship with that observed by Wang and Raj,[21] who first reported ceramic tensile superplasticity using a lithium–alumina–silicate-based glass ceramic (Corning 9608 glass). Tensile elongation of up to 135% was obtained in their experiments, conducted at 1150°C, which was accompanied by a substantial strain-hardening behavior. In this case, the strain hardening was caused primarily by a coarsening of the equiaxed microstructure, and secondarily by the increased viscosity of the glass phase over time due to compositional changes. In this sense, there was a genuine increase of the flow stress on the glass–ceramic interface. By comparison, we believe the aligned, whiskerlike microstructure found here is capable of causing strain hardening without raising the local interfacial flow stress. Thus, a higher ductility is theoretically possible.

(2) Texture Development

The geometrical model for texture development with elongated grains, though fundamentally different from that usually observed in slip-controlled texture development, is quite general and should be suitable for many applications. (Slip and dislocation activities are absent in the present case in view of the very low stresses, very high rate sensitivity, and the very low homologous temperature for silicon nitride.) The prerequisite of the model is a rodlike morphology for the grain and the absence of impediment for rotation due to any physical constraint, such as that exerted by an interlocking network. The presence of a liquid phase with a substantially lower deformation resistance is helpful in this context, as long as the tractions which effect the grain rotation can still be transmitted through the liquid to the side faces of the elongated grains. At the strain rate employed in this study, we envision no liquid/solid slippage to take place on the liquid–grain interface. Thus, the geometrical model is entirely adequate for describing texture development. We have seen in Fig. 9 that the resultant texture by this mechanism can be extremely strong, more than any other deformation texture reported for the same and other families of materials in the ceramic literature.[22–29]

Other applications of the model may be found in cases where the included phases are elongated. Indeed, an independent study of our colleague Hosford[30] has shown that the deformation texture of a rodlike polymetric second phase is also in accord with the present model. The common observation of rod texturing by a shear or uniaxial flow is likewise describable by the same picture, although at high flow velocities slippage will occur at the liquid–solid interface, and the geometric model will overestimate the texturing effect.

(3) Kinetics of Grain Growth of Silicon Nitride

Anisotropic grain growth of β-silicon nitride is usually regarded as a variation of the Ostwald ripening phenomenon for particles in a liquid surrounding.[14] Such a model, which predicts a growth exponent of 3, can be used to understand the growth kinetics in the [001] (long) direction, which has a rounded grain surface that facilitates diffusional growth without interface barrier.[6] The growth in the transverse [210] direction, which has a flat prismatic surface except for occasional ledges, is more sluggish for lack of growth sites. Based on high-resolution TEM observations, grain growth has been suggested to proceed by a spiral dislocation mechanism which is in turn coupled to some of the growth steps in the axial direction.[6] The growth anisotropy can then be explained in terms of the geometric factor pertaining to the ledge (dislocation) density. Further modification of such a picture, by allowing for an imperfect coupling between the axial and lateral growth, is also possible if the growth kinetics and geometry of spiral dislocations are considered in more detail.

The present investigation reveals that a significantly enhanced grain growth, in essentially the same anisotropic manner, can occur at a much lower temperature (1550°C) due to the assistance of a tensile plastic strain. We have suggested two sources of the enhanced growth: grain coalescence and unimpingement. The direct micrographical evidence for the former is presented. Such a mechanism, however, is important only in a highly aligned microstructure and is not expected to contribute much to static grain growth in sintered silicon nitride. On the other hand, the unimpingement mechanism, which points to the importance of the constraint effect of interlocking grains, could have broader implications for static grain growth.

To independently verify the importance of the constraint effect, it would be desirable to compare the growth kinetics of β′-SiAlON grains in solid–liquid assemblages with and without impingement. Such data are not available in the literature, to our knowledge, since almost all of the microstructures published clearly show grain impingement even when a large fraction of liquid (say, 50 wt%) was used. The impingement also occurs at a very early stage, even for fine-grained materials, as is evident from Fig. 5, so that the resultant microstructure is quite resistant to coarsening. While deformation can induce grain growth, we found that at higher displacement rates, e.g., $V = 0.0042$ mm/s ($\dot{\varepsilon}_0 = 0.0003\ s^{-1}$), relatively little anistropic grain growth occurred, even after 70% tensile elongation at 1550°C for 38 min. (The crystallographic texture developed in this case was also moderate.) Noting that the time elapsed in this experiment was only one-tenth of that for the specimen shown in Figs. 1, 2, 6, and 9, we believe the deformation time was too short for anisotropic grain shapes to develop. This in turn caused a loss of grain alignment and the attendant grain coalescence. (The above strain rate of $3 \times 10^{-4}\ s^{-1}$ might be considered equal to the instrinsic growth rate of unconstrained silicon nitride grains at 1550°C.) It is also worth mentioning that, without a significant anisotropic grain growth, the whisker reinforcement effect on the composite was largely lost, as reflected in the relatively flat stress–strain curve recorded in this case (Fig. 2). This last example clearly demonstrates that it is grain alignment and, by implication, grain unimpingement that

triggers enhanced grain growth. A large strain, without grain rotation, is itself insufficient for relieving the constraint.

VI. Conclusions

(1) A fine-grained liquid-constraining β′-SiAlON was found to be superplastic around 1550°C at a strain rate below $3 \times 10^{-4}\ s^{-1}$. Elongations over 230% have been achieved. The measured strain rate sensitivity was 0.68, and thermal activation energy was 940 kJ/mol.

(2) Although the initial microstructure was stable against annealing at the test temperatures, it developed a strong texture and coarsened anisotropically during deformation, with the long-grain axis aligned parallel to the tension direction.

(3) The deformation texture was due to grain reorientation in accordance to the strain field. It is suggested that the presence of a viscous liquid facilitates the grain rotation without hindrance. A geometrical model has been developed which accurately predicts the observed orientation distribution and the extent of the alignment.

(4) The much faster dynamic grain growth, which is up to 5 times faster than static grain growth, can be explained by grain unimpingement and grain coalescence during deformation. Direct microstructural evidence of the latter was found in the wavy grain surfaces uncharacteristic of silicon nitride.

(5) Superplastic flow behavior of this glass-containing ceramic can be described by a rheological model after taking into account the grain alignment/growth development. A pronounced "fiber-reinforcement" effect has been identified. Although this gives rise to extreme strain hardening, fracture is, nevertheless, delayed until a very large elongation. Therefore, quite uniquely, the deformation texture enhances the tensile ductility.

Acknowledgments: We are grateful to Professors W. F. Hosford and T. Y. Tien, who suggested the coalescence mechanism, for enlightening discussions.

References

[1]D. S. Wilkinson and C. H. Caceres, "On the Mechanism of Strain-Enhanced Grain Growth during Superplastic Deformation," *Acta Metall.*, **32**, 1335–45 (1984).

[2]I-W. Chen and L.A. Xue, "Development of Superplastic Structural Ceramics," *J. Am. Ceram. Soc.*, **73** [9] 2585–609 (1990).

[3]I-W. Chen and S.-L. Hwang, "Shear Thickening Creep in Superplastic Silicon Nitrides," *J. Am. Ceram. Soc.*, **75** [5] 1073–79 (1992).

[4]E. Tani, S. Umebayashi, K. Kishi, and M. Nishijma, "Gas Pressure Sintering of Si_3N_4 with Concurrent Addition of Al_2O_3 and 5 wt% Rare Earth Oxide—High Fracture Toughness Si_3N_4 with Fiber-Like Structure," *Am. Ceram. Soc. Bull.*, **65** [9] 1311–15 (1986).

[5]G. Ziegler, J. Heinrich, and G. Wotting, "Review: Relationship between Processing, Microstructure and Properties of Dense and Reaction-Bonded Silicon Nitride," *J. Mater. Sci.*, **22**, 3041–86 (1987).

[6]M. Hwang, T. Y. Tien, and I-W. Chen, "Anisotropic Grain Growth in Final Stage Sintering of Silicon Nitride Ceramics"; pp. 1034–39 in *Sintering '87, Proceedings of 4th International Symposium on Science and Technology of Sintering*, Vol. 2, Tokyo, Japan, November 4–7, 1987. Edited by S. S. Somiya, M. Shimada, M. Yoshimura, and R. Watanabe. Elsevier Applied Science, London, U.K., 1988.

[7]D. D. Lee, S. L. Kang, and D. N. Yoon, "Mechanism of Grain Growth and α–β′ Transformation during Liquid-Phase Sintering of β′-SiAlON," *J. Am. Ceram. Soc.*, **71** [9] 803–806 (1988).

[8]M. Mitomo, M. Tsutsumi, H. Tanaka, S. Venosone, and F. Saito, "Grain Growth during Gas-Pressure Sintering of β-Silicon Nitride," *J. Am. Ceram. Soc.*, **73** [8] 2441–45 (1990).

[9]K.-R. Lai and T. Y. Tien, "Kinetics of β-Si_3N_4 Grain Growth under High Nitrogen Pressure," submitted to *J. Am. Ceram. Soc.*

[10]F. Wakai, Y. Kodama, S. Sakaguchi, N. Murayama, K. Izaki, and K. Niihara, "A Superplastic Covalent Composite," *Nature (London)*, **344** [6265] 421–23 (1990).

[11]H. J. Bunge, "Method of ODF Calculation"; pp. 3–16 in *Textures of Materials, Proceedings of Fifth International Conference on Textures of Materials*, Vol. 1. Edited by G. Gottstein and K. Lücke. Springer-Verlag, Berlin, New York, 1978.

[12]L. J. Gauckler, J. Weiss, T. Y. Tien, and G. Petzow, "Insolubility of Mg in β-Si_3N_4 in the System Al–Mg–Si–O–N," *J. Am. Ceram. Soc.*, **61** [9–10] 397–98 (1978).

[13]S. Takajo, W. A. Kaysser, and G. Petzow, "Analysis of Particle Growth by Coalescence during Liquid Phase Sintering," *Acta Metall.*, **32** [1] 107–13 (1984).

[14]C. Wagner, "Theory of Precipitate Change by Redistribution," *Z. Elektrochem.*, **65**, 581–91 (1961).

[15]I-W. Chen, "Superplastic Flow of Two-Phase Alloys"; pp. 5.1–5.20 in *Superplasticity*. Edited by B. Baudelet and M. Suery. Editions du CNRS, Paris, France, 1985.

[16]C. K. Yoon and I-W. Chen, "Superplastic Flow of Two-Phase Ceramics Containing Rigid Inclusions–Zirconia/Mullite Composites," *J. Am. Ceram. Soc.*, **73** [6] 1555–65 (1990).

[17]T. G. Nieh and J. Wadsworth, "Superplasticity in Fine-Grained YTZ Composites"; in Ceramic Transactions, Vol. 19, *Advanced Composite Materials*. Edited by M. D. Sacks. American Ceramic Society, Westerville, OH, 1991.

[18]T. Kuroishi, K. Uno, and F. Wakai, "Characterization of Superplastic ZrO_2-Toughened Al_2O_3 Prepared by Slip Casting"; pp. 267–74 in *Superplasticity, Proceedings of the MRS International Meeting of Advanced Materials*, Vol. 7. Edited by M. Doyama, S. Somiya, and R. H. Champ. Materials Research Society, Pittsburgh, PA, 1989.

[19]C. Carry and A. Mocellin, "Examples of Superplastic Forming Fine-Grained Al_2O_3 and ZrO_2 Ceramics"; pp. 1043–52 in *Materials Science Monographs 38A, High Tech Ceramics*. Edited by P. Vincenzini. Elsevier Science Publishers, Amsterdam, Netherlands, 1987.

[20]F. Wakai, "Superplasticity of Zirconia-Toughened Ceramics"; Ph.D. Thesis. Kyoto University, Kyoto, Japan, 1988.

[21]J.-G. Wang and R. Raj, "Mechanism of Superplastic Flow in a Fine-Grained Ceramic Containing Some Liquid Phase," *J. Am. Ceram. Soc.*, **67** [6] 399–409 (1984).

[22]Y. Goto, H. Ohta, and M. Komatsu, "Preferred Orientation and Mechanical Properties of Pressureless Sintered Silicon Nitride," *Yogyo Kyokaishi*, **94** [1] 167–71 (1986).

[23]H. Knock, K. A. Schwetz, and A. Lopps, "Microstructural Development in Silicon Nitride"; pp. 381–92 in *Progress in Nitrogen Ceramics*. Edited by F. L. Riley. Noordhoff, Leyden, Netherlands, 1983.

[24]K. J. Bowman, P. E. Reyes-Morel, and I-W. Chen, "Texture from Deformation of Zirconia-Containing Ceramics"; pp. 811 in *ICOTOM, 8th International Conference on Textures of Materials*, Santa Fe, NM, September 20–25, 1987. Edited by J. S. Kallend and G. Gottstein. The Metallurgical Society, Warrendale, PA, 1988.

[25]T. Takenaka and K. Sakata, "Grain Orientation and Electrical Properties of Hot-Forged $Bi_4Ti_3O_{12}$ Ceramics," *Jpn. J. Appl. Phys.*, **19**, 31–39 (1980).

[26]I-W. Chen, X. Wu, S. Keating, C. Y. Keating, P. Johnson, and T. Y. Tien, "Texture Development in $YBa_2Cu_3O_x$ by Hot Extrusion and Hot-Pressing," *J. Am. Ceram. Soc.*, **70** [12] C-388 (1987).

[27]H. R. Wnek, *Preferred Orientation in Deformed Metals and Rocks: An Introduction to Modern Texture Analysis*. Academic Press, New York, 1985.

[28]F. Lee and K. J. Bowman, "Texture and Anisotropy in Silicon Nitride," *J. Am. Ceram. Soc.*, **75** [7] 1748–55 (1992).

[29]K. J. Bowman and I-W. Chen, "Transformation Textures in Zirconia," submitted to *J. Am. Ceram. Soc.*

[30]W. F. Hosford, *Mechanics of Crystals and Textured Polycrystals*, Oxford University Press, Oxford, U.K., in press (1991).